Earth and Planetary Science Letters 424 (2015) 280–294

Contents lists available at ScienceDirect

Earth and Planetary Science Letters

www.elsevier.com/locate/epsl

The effects of composition and temperature on chalcophile and lithophile element partitioning into magmatic sulphides

Ekaterina S. Kiseeva *, Bernard J. Wood

Department of Earth Sciences, University of Oxford, Oxford OX1 3AN, UK

ARTICLE INFO

Article history:
Received 8 December 2014
Received in revised form 28 April 2015
Accepted 5 May 2015
Available online 28 May 2015
Editor: J. Brodholt

Keywords:
chalcophile element partitioning
thermodynamic modelling
MORB generation

ABSTRACT

We develop a comprehensive model to describe trace and minor element partitioning between sulphide liquids and anhydrous silicate liquids of approximately basaltic composition. We are able thereby to account completely for the effects of temperature and sulphide composition on the partitioning of Ag, Cd, Co, Cr, Cu, Ga, Ge, In, Mn, Ni, Pb, Sb, Ti, Tl, V and Zn. The model was developed from partitioning experiments performed in a piston-cylinder apparatus at 1.5 GPa and 1300 to 1700 °C with sulphide compositions covering the quaternary FeS–NiS–$CuS_{0.5}$–FeO.

Partitioning of most elements is a strong function of the oxygen (or FeO) content of the sulphide. This increases linearly with the FeO content of the silicate melt and decreases with Ni content of the sulphide. As expected, lithophile elements partition more strongly into sulphide as its oxygen content increases, while chalcophile elements enter sulphide less readily with increasing oxygen. We parameterised the effects by using the ε-model of non-ideal interactions in metallic liquids. The resulting equation for partition coefficient of an element M between sulphide and silicate liquids can be expressed as

$$\log D_M^{sulph/sil} = A + \frac{B}{T} - \frac{n}{2}\log[\mathrm{FeO}]_{corr} + \frac{1673}{T}\left[\varepsilon^{\mathrm{FeO}}_{\mathrm{MS}_{n/2}}\log(1-x_{\mathrm{FeO}}) + \varepsilon^{\mathrm{NiS}}_{\mathrm{MS}_{n/2}}\log(1-x_{\mathrm{NiS}}) + \varepsilon^{\mathrm{CuS_{0.5}}}_{\mathrm{MS}_{n/2}}\log(1-x_{\mathrm{CuS_{0.5}}})\right]$$

where A is a constant related to the entropy change of the partitioning reaction, B is a constant related to its enthalpy and n is the valency of the element of interest. Interaction parameters $\varepsilon^{\mathrm{FeO}}$, $\varepsilon^{\mathrm{NiS}}$ and $\varepsilon^{\mathrm{CuS_{0.5}}}$ refer to non-ideal interactions between trace element and matrix, x_{FeO}, x_{NiS}, $x_{\mathrm{CuS_{0.5}}}$ and x_{FeS} are mole fractions of FeO, NiS, and $CuS_{0.5}$ in sulphide and FeO_{corr} is FeO content of silicate liquid (wt%) corrected for the ideal activity of FeS in the sulphide as follows:

$$[\mathrm{FeO}]_{corrected} = \frac{[\mathrm{FeO}]_{silicate}}{[\mathrm{Fe}/(\mathrm{Fe}+\mathrm{Ni}+\mathrm{Cu})]_{sulph}}$$

We find, for most elements, that the effect of Ni and Cu on partitioning is significantly smaller than the effect of oxygen. The effects of temperature are greatest for Ni, Cu and Ag.

We used our model to calculate the amount of sulphide liquid precipitated along the liquid line of descent of MORB melts and find that 70% of silicate crystallisation is accompanied by ~0.23% of sulphide precipitation. The latter is sufficient to control the melt concentrations of chalcophile elements such as Cu, Ag and Pb. Our partition coefficients and observed chalcophile element concentrations in MORB glasses were used to estimate sulphur solubility in MORB liquids. We obtained between ~800 ppm (for primitive MORB) and ~2000 ppm (for evolved MORB), values in reasonable agreement with experimentally-derived models. The experimental data also enable us to reconsider Ce/Pb and Nd/Pb ratios in MORB. We find that constant Ce/Pb and Nd/Pb ratios of 25 and 20, respectively, can be achieved during fractional crystallisation of magmas generated by 10% melting of depleted mantle provided the latter contains >100 ppm S and about 650 ppm Ce, 550 ppm Nd and 27.5 ppb Pb.

Finally, we investigated the hypothesis that the pattern of chalcophile element abundances in the mantle was established by segregation of a late sulphide matte. Taking the elements Cu, Ag, Pb and Zn as

* Corresponding author.
E-mail addresses: kate.kiseeva@earth.ox.ac.uk (E.S. Kiseeva), berniew@earth.ox.ac.uk (B.J. Wood).

http://dx.doi.org/10.1016/j.epsl.2015.05.012

examples we find that the Pb/Zn and Cu/Ag ratios of the mantle can, in principle, be explained by segregation of ~0.4% sulphide matte to the core.

1. Introduction

Sulphides, despite their low modal abundances in most rocks, have a propensity to concentrate a number of elements which are of geochemical and economic importance. These include Pt-group elements, Cd, In, Cu, Ag and Pb which means that they are major carriers of these elements in mantle and crust. The decreasing solubility of S in silicate melts with decreasing temperature (Holzheid and Grove, 2002) and the common presence of immiscible sulphide globules in basaltic magmas imply that MORB are generally at sulphide saturation throughout their path of ascent to the surface. This has profound effects on the Ce/Pb and Nd/Pb ratios of N-MORB which appear to be approximately constant at ~25 and ~20 respectively (Hart and Gaetani, 2006). Since Pb is much more incompatible in mantle silicates than Ce and Nd, the only way of keeping these ratios constant is to remove a small fraction of chalcophile Pb in precipitating sulphide. We show below how this and related observations can be used to constrain the extent of sulphide precipitation and sulphide composition during fractionation of MORB melts. The ability of sulphides to concentrate chalcophile elements is economically important in the context of, for example, Ni and PGE-rich magmatic sulphide deposits, and high temperature copper porphyry deposits. Many other chalcophile elements (Cd and In for example) are also of economic importance, which makes the interpretation and understanding of their geochemical behaviour of considerable value.

Sulphide and chalcophile elements have played important roles in the accretion and differentiation of the Earth. S is, for an element of its volatility, of very low abundance in the silicate Earth (Dreibus and Palme, 1996). Dreibus and Palme (1996) compared the abundance of S with that of Zn, an element of similar volatility and estimated that about 99% of Earth's sulphur resides in the core. This probably arose from a combination of dissolution in the segregating Fe-rich core and addition to the core of a late sulphide matte (O'Neill, 1991; Wood and Halliday, 2005). The effects of such a matte would be to remove large fractions of chalcophile elements to the Earth's core with corresponding increase in ratios such as U/Pb in the silicate Earth (Hart and Gaetani, 2006). Hart and Gaetani (2006) also suggested that the "lead paradox", the observation that silicate Earth lies to the right of the "geochron" on a $^{207}Pb/^{204}Pb$ vs $^{206}Pb/^{204}Pb$ diagram could be due to ongoing Pb dissolution, as sulphide, into the core. Quantitative interpretation of this possibility requires an accurate model of Pb sulphide–silicate partition coefficients, however.

A plot of elemental abundance in the silicate Earth versus temperature of 50% condensation from a gas of solar nebula composition (Lodders, 2003) shows that the silicate Earth is strongly depleted in chalcophile elements such as Ag, Se, Ge, Bi, Tl, Cd and Sb relative to lithophile elements of similar volatility. Segregation of the putative "Hadean matte" to the core late in accretion is a plausible explanation but cannot be quantitatively explored without a reliable model for sulphide–silicate partitioning of the chalcophile elements.

Experimental liquid sulphide–liquid silicate partitioning studies reported in the literature have explored the behaviour of a range of chalcophile elements (Cu, Co, Pb, Bi, Ag, V, Ni, Zn, As, Mo, Sn, Sb, W, Au) under different oxygen and sulphur fugacity conditions (Gaetani and Grove, 1997; Holzheid and Lodders, 2001; Li and Audétat, 2012; Li, 2014; Mungall and Brenan, 2014; Ripley et al., 2002; Wood et al., 2008). This is because the partitioning of a given element is controlled by the ratio of oxygen to sulphur fugacities as can be seen from the equilibrium:

$$\underset{\text{silicate}}{MO_{n/2}} + \tfrac{n}{4}S_2 = \underset{\text{sulphide}}{MS_{n/2}} + \tfrac{n}{4}O_2 \quad (1)$$

In Eq. (1) n is the valence of element M. Although a perfectly valid experimental approach, the utility of data at known oxygen to sulphur fugacity ratio is questionable, because it is impossible to determine the ratio of oxygen to sulphur fugacities very accurately for natural samples. This makes extrapolation from experiment to nature rather uncertain.

Our approach (Kiseeva and Wood, 2013) is to circumvent the need to define oxygen and sulphur fugacities by treating chalcophile element partitioning in terms of an exchange reaction between element M in the silicate melt and Fe in the sulphide liquid:

$$\underset{\text{silicate}}{MO_{n/2}} + \tfrac{n}{2}\underset{\text{sulphide}}{FeS} = \underset{\text{sulphide}}{MS_{n/2}} + \tfrac{n}{2}\underset{\text{silicate}}{FeO} \quad (2)$$

Using this approach we were able to parameterise the sulphide–silicate partition coefficients of a number of chalcophile elements as a function of the FeO content of the silicate liquid in equilibrium with the liquid sulphide (Kiseeva and Wood, 2013).

Partition coefficients may be defined as

$$D_M^{sulph/sil} = \frac{C_M^{sulph}}{C_M^{sil}} \quad (3)$$

where D is the partition coefficient of the element M between sulphide and silicate and C is concentration of this element measured in ppm in each phase.

The relationship between partition coefficient and FeO content of the silicate liquid could, we showed, be represented as follows:

$$\log D_M^{sulph/sil} \approx A + \frac{n}{2}\log[FeO] \quad (4)$$

where A is a constant related to the free energy of Fe-M exchange, n depends on the valency of element M and [FeO] is the concentration of FeO in the silicate liquid in wt%.

Kiseeva and Wood (2013) demonstrated the validity of the approach embodied by Eq. (4) for a number of chalcophile and moderately chalcophile elements at constant temperature (1400 °C), pressure (1.5 GPa) and essentially constant sulphide and silicate liquid compositions. Although there were sufficient thermodynamic data for us to calculate the theoretical effect of temperature for some elements, our initial approach was to test Eq. (4) under isothermal and isobaric conditions. Demonstration that it is valid provides a framework for extensions to determine the influences of pressure, temperature and liquid composition.

We consider, initially, that the effects of pressure in the region of magma genesis and fractionation on Earth (0–3 GPa approximately) are subordinate to those of temperature. Literature data on sulphide–silicate melt partitioning of Ni and Co (Li and Agee, 1996) show that the change in partition coefficients on increasing pressure from 2 to 10 GPa is very small. Undetectable pressure effects between 0 and 24 GPa were also obtained by Wood (unpublished data) for sulphide–silicate partitioning of Pb, V, Sb and Tl. Thermodynamic data by Barin et al. (1989), on the other hand imply strong temperature effects on sulphide–silicate partitioning of Cu, Ni and Pb which requires that the temperature effects be thoroughly explored. Furthermore, given that most natural sulphides

Table 1
Experimental results.

Run No.	Starting composition	Duration (h)	Temperature (°C)
Cu1-1	MORB + FeS + 5.4%Cu_2O + 0.3%NiO	2	1400
Cu2-1	MORB + FeS + 7.4%Cu_2O + 0.4%NiO	2	1400
Cu3-1	MORB + FeS + 9.9%Cu_2O + 0.2%NiO	2	1400
Cu4-1	MORB + FeS + 2.5%Cu_2O + 0.2%NiO	3	1400
Cu5-1	MORB + FeS + 5%Cu_2S	2	1400
Cu6-1	MORB + FeS + 7.2%Cu_2S + 0.5%NiS	2	1400
Cu7-1	MORB + FeS + 9.9%Cu_2S + 0.6%NiS	2	1400
Cu8-1	MORB + FeS + 2.7%Cu_2S + 1.2%NiS	2	1400
Cu8-2	MORB + FeS + 2.7%Cu_2S + 1.2%NiS	2	1400
Cu9-1	MORB + FeS + 4.9%Cu_2S + 5.4%NiS	2	1400
Cu10-1	MORB + FeS + 2.1%Cu_2S + 0.7%NiS + 20%FeO	1.5	1400
Cu11-1	CMAS + FeS + 2.2%Cu_2S + 0.5%NiS	2	1400
Cu12-1	MORB + FeS + Cu_2O(tr) + 11.5%NiS + 25%FeO	2	1400
KK12-2	MORB + FeS + NiS(tr) + 33%FeO	1.5	1400
Ni3-1	CMAS + FeS + Cu_2O(tr) + 23%Ni_3S_2 + 3.4%FeO	2	1400
Ni5-2	MORB + FeS + 23%Cu_2S + 27%Ni_3S_2	0.25	1400
Ni6-2	MORB + FeS + 24%Ni_3S_2	0.5	1400
Ni7-1	MORB + FeS + 24.8%Ni_3S_2 + 6.3%FeO	0.17	1400
KK4-6	MORB + FeS + 0.5%NiS	0.5	1650
KK4-7	MORB + FeS + 0.5%NiS	0.5	1650
KK4-8	MORB + FeS + 0.5%NiS	2	1300
KK4-9	MORB + FeS + 0.5%NiS	1	1500
KK4-10	MORB + FeS + 0.5%NiS	3	1300
KK15-6	MORB + FeS + NiS(tr) + 20%FeO	0.5	1650
KK16-3	CMAS + FeS + 0.5%NiS	0.5	1650
Cu10-2	MORB + FeS + 2.1%Cu_2S + 0.7%NiS + 20%FeO	0.5	1650
Cu11-2	CMAS + FeS + 2.2%Cu_2S + 0.5%NiS	0.65	1600
Cu11-3	CMAS + FeS + 2.2%Cu_2S + 0.5%NiS	0.2	1700
Cu11-5	CMAS + FeS + 2.2%Cu_2S + 0.5%NiS	1	1500

Graphite capsules were used for all runs. NiS(tr) – less than 0.5% added in the bulk starting mixture.
MORB – taken from Falloon and Green, 1987 (Table 1, column 2). CMAS – $Fo_{22}Di_{28}An_{50}$.
All runs were doped with trace element mixture TR (see Kiseeva and Wood, 2013).

are solid solutions between FeS, NiS and Cu_2S, it is also important to test compositional effects on trace element partitioning, by varying Cu and Ni contents of sulphide liquids. The principal aims of this study were, therefore, to establish the effects of temperature and sulphide melt composition on sulphide–silicate melt partitioning of 16 elements: Ag, Cd, Co, Cr, Cu, Ga, Ge, In, Mn, Ni, Pb, Sb, Ti, Tl, V and Zn. In the course of our experimental program, however, we established that the oxygen content of the sulphide has a profound effect on the partitioning of many of these elements. We therefore also established and parameterised the "oxygen effect" for these 16 elements partitioning between sulphide and silicate melts.

2. Experimental methods

We used, as starting materials, ~50:50 mixtures of synthetic sulphide and synthetic silicate, by weight. Sulphide components were principally mixtures of analytical grade Cu_2S, NiS (or Ni_3S_2) and FeS. For some of the experimental compositions (see Table 1) Cu_2O and NiO were used as sources of Cu and Ni instead of Cu_2S and NiS. No textural differences were observed between experiments employing oxides of these 2 elements and those in which sulphides were used. The silicate constituents were the same as those used in our previous study (Kiseeva and Wood, 2013) with silicate being added either as fused (at IW + 2 log units) synthetic MORB (Falloon and Green, 1987) or as a fused CaO–MgO–Al_2O_3–SiO_2 composition close to the 1.5 GPa eutectic composition in the system anorthite–diopside–forsterite ($An_{50}Di_{28}Fo_{22}$) (Presnall et al., 1978).

Mixtures were prepared in the same way as reported by Kiseeva and Wood (2013). After drying in the oven at ~110 °C overnight, they were loaded into 3 mm O.D., 1 mm I.D. graphite capsules and run for 1.5–3 h at 1400 °C and 1.5 GPa in an end-loaded Boyd-England-type piston cylinder apparatus at the University of Oxford. The previous set of experiments (Kiseeva and Wood, 2013) demonstrated that 0.5 h were sufficient for the equilibrium to be achieved at 1400 °C and earlier work established metal–silicate equilibrium in ~3 min at 1650 °C (Tuff et al., 2011). The duration of high-temperature runs (between 1500 and 1700 °C) was therefore between 1 h and 12 min with shortest run duration at 1700 °C.

We did not observe any significant loss of Cu in our experiments, although up to 50% of Ni was lost when Ni was added as NiO or NiS. Ni-loss from graphite capsules was previously reported by Matzen et al. (2013) and may have occurred, possibly due to formation of volatile Ni-carbonyl ($Ni(CO)_4$) during the experiment. To minimise Ni-loss, experiments with high concentrations of Ni (denoted NiI-J, in Table 1) generally had shorter durations (10–30 min). No Ni-loss was encountered for the experiments with Ni added as Ni_3S_2 including Ni3-1, which was of 2 h duration.

All the experiments quenched to homogeneous silicate and sulphide liquids (in the case of Fe- and Ni-rich sulphides). Cu-rich sulphides tend to quench to heterogeneous intergrowths (Supplementary Fig. 5). We minimised the analytical standard error on these by performing more than 40 microprobe analyses of sulphide blobs from each experiment. The average value for WDS and LA-ICPMS measurements on Cu and Ni was generally within 10% relative except as noted below.

The experimental products were analysed using a JEOL JXA8600 electron microprobe at the Department of Archaeology at the University of Oxford. WDS analyses were conducted using a 15 kV accelerating voltage and 20 to 40 nA beam current with a defocused 10 micron spot to improve averaging of both silicate and sulphide phases. The detailed description of analytical procedure and standards can be found in Kiseeva and Wood (2013). Trace-element concentrations of the co-existing silicate glasses and sulphides were determined on experimental products using LA-ICPMS. The following masses were counted: ^{29}Si, ^{44}Ca, ^{47}Ti, ^{51}V, ^{53}Cr, ^{55}Mn, ^{57}Fe, ^{59}Co, ^{60}Ni, ^{65}Cu, ^{66}Zn, ^{71}Ga, ^{74}Ge, ^{107}Ag, ^{111}Cd, ^{115}In, ^{121}Sb,

^{205}Tl, ^{208}Pb, with yields calibrated on NIST 610 glass standard as the primary standard. We used Fe as the internal standard for the sulphide analyses and Si for the silicates. Measurements were made using a Perkin Elmer Nexion quadrupole mass spectrometer coupled to a New Wave Research UP213 Nd:YAG laser at the University of Oxford. Beam diameters of 50 μm were used for both silicate and sulphide phases (see Supplementary Information).

In our previous study (Kiseeva and Wood, 2013), we reported no systematic deviations between Ni and Cu measurements made by LA-ICPMS and WDS for sulphides with Cu and Ni contents up to 0.5 wt% and 14 wt%, respectively. Additional experiments with significantly higher concentrations of Cu in the sulphide liquid (4–15 wt%) show some deviation between the 2 techniques when there is more than 7 wt% Cu in sulphide (Supplementary Fig. 1). At concentrations above 7 wt% Cu in sulphide the systematic offset means that the LA-ICPMS method yields approximately 0.8 times the microprobe concentration. Because the quenched sulphides are heterogeneous, however, the microprobe analyses always have much higher standard deviations. Therefore in order to compute Cu partition coefficients at high Cu content we used the LA-ICPMS data for sulphides and applied an empirical correction factor of 1.25. This accounts for any systematic error accumulating from the differences in concentrations and matrices between standards and unknowns. No other corrections were applied and LA-ICPMS values were used for all of the trace elements.

3. Results

Major element compositions of experimental products are presented in Tables 2 and 3 and partition coefficient values in Table 4. Trace element compositions are presented in Supplementary Tables 1 and 2. All of the trace elements were above detection limit, including Ti, which was not deliberately added into the CMAS composition, but was present as a contaminant.

3.1. Oxygen solubility in sulphide and its effect on sulphide–silicate partitioning

Oxygen is a significant component of immiscible sulphides in MORB and has important impacts on partitioning in magmatic sulphide deposits (Czamanske and Moore, 1977; Fonseca et al., 2008; Roy-Barman et al., 1998). Sulphide blobs recovered from MORB glasses contain on average about 2 wt% oxygen (Roy-Barman et al., 1998). At equilibrium, the activity of FeO (a_{FeO}) in silicate and sulphide liquids must be identical which means that the oxygen content of the sulphide melt must increase with increasing FeO content of the silicate liquid. Empirically we find:

$$\mathrm{O\,(wt\%\text{-}sulphide)} = 0.24\,\mathrm{FeO\,(wt\%\text{-}silicate)} \quad (5)$$

The slope of 0.24 is close to the value of 0.223 calculated for the case where the ratio of activity coefficients for FeO in silicate and sulphide is 1. Since FeO activity coefficients in silicate melts are close to 1 (O'Neill and Eggins, 2002) and FeS–FeO melts exhibit only small negative deviations from ideality (Nagamori and Yazawa, 2001) this agreement between observed and "ideal" slopes is as expected.

In sulphides with high Ni-contents, we observe significantly lower oxygen contents than would be calculated from Eq. (5) (Fig. 1a). For example, sulphide melt from experiment Ni3-1 with 35 wt% Ni in sulphide contains only 0.5 wt% oxygen instead of the expected 2 wt%. This can be explained by the known decrease in oxygen solubility in sulphide with increasing Ni-content (Fonseca et al., 2008; Kress, 2007; Yoshiki-Gravelsins and Toguri, 1993). Our limited dataset is not sufficient to parameterise this dependence accurately, but according to Yoshiki-Gravelsins and Togure (1993),

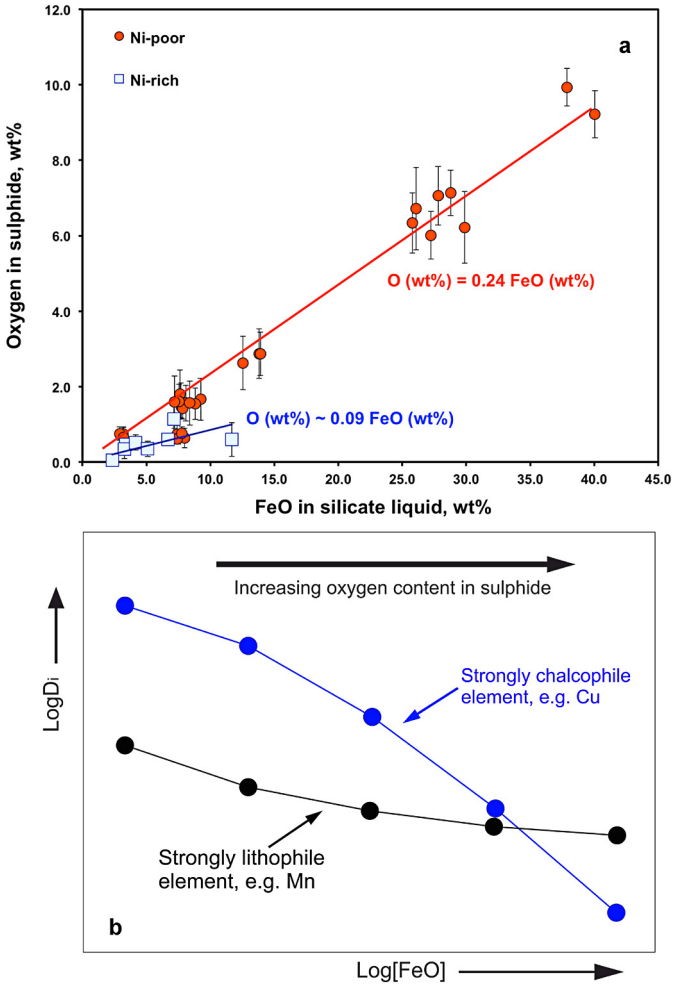

Fig. 1. (a) Oxygen content of sulphide melt as a function of the FeO content of the silicate liquid. Error bars refer to ±1 standard deviation (on 25–94 analyses, see Table 3). Additional data from Kiseeva and Wood (2013). (b) Expected behaviour of lithophile and chalcophile elements partitioning into sulphide as a function of the FeO content of the silicate liquid (and hence the O content of sulphide).

the relationship is close to parabolic. We therefore apply a correction based on the concentration of Ni in sulphide as follows:

$$\mathrm{O}_{calc}\ (\mathrm{wt\%}) = 0.24\mathrm{FeO}\left(1 - \frac{\mathrm{Ni}}{\mathrm{Ni}+\mathrm{Cu}+\mathrm{Fe}}\right)^2 \quad (6)$$

Eq. (6) accurately reproduces the oxygen contents of our experimentally-produced sulphides (Supplementary Fig. 3). Fonseca et al. (2008) suggested that, in addition to the dramatic effect of Ni content of the sulphide on its oxygen content there is also a slight effect of Cu content. We do not, however, observe any change in O solubility with Cu contents up to 16 wt% so we have chosen, for simplicity, to ignore any possible effect.

The need to parameterise the oxygen content of sulphide melt comes from its effect on sulphide–silicate partitioning. In theory, the slope of $\log D_M$ vs log[FeO], should reflect the valency of M – Eq. (4) – with a slope of −0.5 for monovalent, −1 for divalent, −1.5 for trivalent elements and so on. With increasing oxygen contents of sulphide however, the partition coefficients of strongly chalcophile elements such as Cu, Ni and Ag, deviate to lower than expected values and generate a downward curvature in the trend (Fig. 1b). The oxygen effect on partitioning of more lithophile elements such as Mn and Ti is opposite. As the oxygen content of the sulphide increases, the slope flattens due to a decrease in the $MS_{n/2}$ activity coefficient in the sulphide

Table 2
Major element compositions of the silicate glass.

Run No.	Cu1-1		Cu2-1		Cu3-1		Cu4-1		Cu5-1		Cu6-1	
n	20	σ	34	σ	65	σ	20	σ	57	σ	20	σ
SiO_2	47.16	0.14	45.44	0.22	45.44	0.15	49.39	0.13	50.01	0.46	48.84	0.23
TiO_2	0.74	0.02	0.73	0.02	0.72	0.02	0.77	0.02	0.81	0.02	0.79	0.03
Al_2O_3	13.86	0.07	14.02	0.07	14.03	0.09	14.57	0.07	15.12	0.28	14.47	0.08
FeO	12.55	0.10	13.80	0.10	13.90	0.11	9.24	0.09	7.62	0.10	8.82	0.14
MgO	9.65	0.05	9.06	0.07	9.04	0.12	10.11	0.05	10.18	0.17	10.40	0.05
CaO	11.47	0.07	10.97	0.06	10.90	0.08	11.81	0.06	12.11	0.24	12.07	0.07
MnO	0.15	0.02	0.15	0.02	0.15	0.02	0.14	0.02	0.13	0.02	0.14	0.01
Na_2O	1.78	0.03	1.70	0.03	1.67	0.03	2.05	0.03	1.96	0.05	2.06	0.03
K_2O	n.m.	–	n.m.	–	n.m.	–	n.m.	–	n.m.	–	n.m.	–
P_2O_5	0.12	0.01	0.11	0.01	0.11	0.01	0.12	0.01	0.12	0.01	0.13	0.01
SO_3	0.57	0.05	0.51	0.09	0.49	0.04	0.45	0.03	0.39	0.03	0.44	0.16
Totals	98.04		96.48		96.45		98.64		98.45		98.15	
Run No.	Cu7-1		Cu8-1		Cu8-2		Cu9-1		Cu10-1		Cu11-1	
n	66	σ	17	σ	37	σ	37	σ	26	σ	23	σ
SiO_2	49.61	0.42	49.34	0.36	48.58	0.45	49.28	0.13	37.60	0.17	45.83	0.12
TiO_2	0.80	0.02	0.79	0.02	0.77	0.02	0.80	0.02	0.59	0.02	b.d.l.	–
Al_2O_3	14.99	0.29	14.75	0.14	14.41	0.27	14.61	0.06	10.77	0.07	17.33	0.05
FeO	7.85	0.16	8.39	0.24	7.45	0.08	7.20	0.09	27.24	0.17	3.21	0.05
MgO	10.23	0.24	10.09	0.07	10.04	0.05	10.21	0.05	7.60	0.05	14.92	0.08
CaO	12.12	0.24	12.12	0.07	12.69	0.23	12.31	0.06	9.45	0.06	17.56	0.10
MnO	0.13	0.02	0.12	0.01	0.12	0.02	0.13	0.02	0.13	0.02	b.d.l.	–
Na_2O	1.93	0.05	1.94	0.03	2.51	0.05	1.88	0.03	1.36	0.03	b.d.l.	–
K_2O	n.m.	–	n.m.	–	n.m.	–	n.m.	–	n.m.	–	n.m.	–
P_2O_5	0.12	0.01	0.13	0.01	0.13	0.01	0.14	0.01	0.05	0.01	b.d.l.	–
SO_3	0.40	0.17	0.49	0.34	0.53	0.04	0.41	0.06	1.47	0.14	0.47	0.04
Totals	98.17		98.16		97.25		96.97		96.27		99.32	
Run No.	Cu12-1		KK12-2		Ni3-1		Ni5-2		Ni6-2		Ni7-1	
n	42	σ	45	σ	33	σ	30	σ	16	σ	31	σ
SiO_2	28.33	0.64	29.54	1.59	44.69	0.50	51.94	0.10	50.94	0.06	46.82	0.09
TiO_2	0.47	0.02	0.44	0.03	n.m.	–	0.84	0.02	0.84	0.02	0.78	0.02
Al_2O_3	9.12	0.21	8.78	0.50	15.46	0.52	15.68	0.04	15.29	0.04	14.05	0.05
FeO	29.88	0.63	37.88	1.57	4.16	0.49	2.33	0.04	5.11	0.06	11.68	0.09
MgO	7.40	0.14	7.16	0.32	15.77	0.64	10.81	0.06	10.56	0.04	9.64	0.06
CaO	16.08	0.40	10.21	0.48	17.52	0.53	13.12	0.06	12.52	0.06	11.53	0.05
MnO	0.12	0.02	0.11	0.02	b.d.l.	–	0.16	0.01	0.15	0.02	0.16	0.02
Na_2O	1.14	0.06	1.25	0.09	b.d.l.	–	1.90	0.04	1.89	0.03	1.70	0.03
K_2O	0.10	0.01	0.10	0.01	n.m.	–	0.15	0.01	0.15	0.01	0.13	0.01
P_2O_5	0.14	0.02	0.16	0.02	n.m.	–	b.d.l.	–	b.d.l.	–	b.d.l.	–
SO_3	1.99	0.78	2.83	0.80	0.20	0.12	0.04	0.05	0.20	0.02	0.25	0.02
Totals	94.75		98.45		97.80		96.97		97.65		96.74	
Run No.	KK4-6		KK4-7		KK4-8		KK4-9		KK4-10		KK15-6	
n	21	σ	27	σ	34	σ	35	σ	22	σ	33	σ
SiO_2	51.27	0.12	48.72	0.22	48.50	0.21	49.16	0.40	48.07	0.30	38.54	0.28
TiO_2	0.79	0.02	0.77	0.01	0.80	0.02	0.81	0.02	0.93	0.03	0.61	0.02
Al_2O_3	15.80	0.09	14.66	0.06	14.81	0.07	15.09	0.14	16.55	0.33	11.80	0.08
FeO	7.13	0.16	8.36	0.17	9.24	0.08	8.74	0.26	9.73	0.11	27.02	0.38
MgO	10.61	0.05	10.60	0.06	10.05	0.08	10.16	0.08	8.09	0.38	7.98	0.07
CaO	12.45	0.05	12.20	0.06	12.06	0.06	12.28	0.11	11.08	0.23	9.63	0.07
MnO	0.11	0.02	0.12	0.02	0.15	0.02	0.14	0.01	0.15	0.02	0.13	0.02
Na_2O	1.99	0.03	1.96	0.03	1.81	0.04	1.92	0.04	2.26	0.14	1.43	0.02
K_2O	n.m.	–	n.m.	–	n.m.	–	n.m.	–	0.21	0.02	n.m.	0.00
P_2O_5	0.13	0.01	0.13	0.01	0.14	0.01	0.13	0.01	0.00	0.00	0.12	0.01
SO_3	0.58	0.15	0.84	0.22	0.42	0.03	0.71	0.25	0.35	0.04	2.03	0.58
Totals	100.85		98.36		97.98		99.14		97.43		99.29	
Run No.	KK16-3		Cu10-2		Cu11-2		Cu11-3		Cu11-5			
n	22	σ	37	σ	29	σ	27	σ	40	σ		
SiO_2	45.64	0.22	38.50	0.23	44.65	0.21	44.90	0.27	44.73	0.16		
TiO_2	b.d.l.	–	0.62	0.02	b.d.l.	–	b.d.l.	–	b.d.l.	–		
Al_2O_3	17.78	0.10	11.28	0.08	17.67	0.08	17.60	0.11	17.54	0.07		
FeO	3.01	0.30	26.40	0.40	3.12	0.23	2.83	0.38	3.49	0.08		
MgO	16.77	0.09	7.80	0.12	16.75	0.08	17.61	0.10	16.57	0.12		
CaO	16.77	0.13	9.14	0.11	16.71	0.09	16.49	0.10	16.67	0.07		
MnO	b.d.l.	–	0.12	0.02	0.02	0.01	0.02	0.01	0.03	0.01		
Na_2O	0.12	0.01	1.38	0.12	0.14	0.01	0.09	0.01	0.07	0.01		
K_2O	n.m.	–	n.m.	–	n.m.	–	n.m.	–	n.m.	–		
P_2O_5	b.d.l.	–	b.d.l.	–	b.d.l.	–	b.d.l.	–	b.d.l.	–		
SO_3	1.17	0.33	1.52	0.36	1.17	0.27	1.48	0.43	0.79	0.10		
Totals	101.27		96.75		100.23		101.02		99.89			

n.m. – not measured.
b.d.l. – below detection limit.

Table 3
Major element compositions of the sulphide.

Run No.	Cu1-1		Cu2-1		Cu3-1		Cu4-1		Cu5-1		Cu6-1	
n	94	σ	66	σ	74	σ	36	σ	44	σ	39	σ
O	2.63	0.71	2.87	0.66	2.87	0.57	1.66	0.56	1.80	0.63	1.55	0.42
S	31.50	1.25	31.22	1.26	30.67	1.39	32.55	0.72	31.87	0.71	31.39	0.86
Fe	53.77	2.62	50.82	3.32	49.10	3.24	58.03	1.74	54.63	1.90	51.86	2.71
Ni	0.60	0.07	1.04	0.08	0.38	0.05	0.46	0.05	0.02	0.01	0.36	0.03
Cu	10.81	2.96	13.34	3.93	16.56	3.91	6.35	2.01	9.95	2.21	13.24	3.13
Total	99.30		99.29		99.58		99.05		98.27		98.40	
Run No.	Cu7-1		Cu8-1		Cu8-2		Cu9-1		Cu10-1		Cu11-1	
n	48	σ	55	σ	24	σ	30	σ	51	σ	39	σ
O	1.42	0.29	1.56	0.58	1.60	0.46	1.59	0.70	6.01	0.63	0.65	0.27
S	31.11	0.57	35.01	0.68	34.85	0.82	32.41	0.62	29.43	0.77	36.46	0.41
Fe	49.25	2.06	56.30	1.30	56.60	1.97	51.92	1.61	60.50	1.75	57.97	0.69
Ni	0.24	0.02	0.89	0.05	0.90	0.05	3.38	0.13	0.51	0.12	0.26	0.02
Cu	16.88	2.47	5.43	1.31	5.15	1.86	7.75	1.81	3.75	1.58	3.65	0.65
Total	98.89		99.20		99.10		97.05		100.20		99.00	
Run No.	Cu12-1		KK12-2		Ni3-1		Ni5-2		Ni6-2		Ni7-1	
n	54	σ	50	σ	46	σ	41	σ	36	σ	37	σ
O	6.22	0.95	9.94	0.42	0.52	0.21	0.04	0.07	0.35	0.20	0.60	0.45
S	27.88	1.10	23.18	0.41	33.15	1.62	24.72	0.78	32.25	0.54	30.91	0.85
Fe	59.41	1.64	67.07	0.60	30.68	5.67	4.39	0.32	32.01	2.48	31.16	3.34
Ni	6.45	1.90	0.23	0.03	35.33	7.00	31.75	7.90	33.98	3.05	36.16	4.06
Cu	0.56	0.11	0.24	0.04	0.66	0.37	38.06	8.97	0.25	0.03	0.36	0.06
Total	100.52		100.66		100.33		98.96		98.84		99.19	
Run No.	KK4-6		KK4-7		KK4-8		KK4-9		KK4-10		KK15-6	
n	9	σ	55	σ	35	σ	60	σ	33	σ	38	σ
O	1.29	0.39	1.67	0.54	2.11	0.40	2.07	0.63	2.22	0.74	6.11	0.90
S	35.71	0.52	35.59	0.63	35.57	0.46	35.19	0.69	36.03	0.85	30.33	1.03
Fe	61.20	0.48	61.29	0.45	61.25	0.35	61.51	0.53	59.71	0.47	64.17	0.58
Ni	0.34	0.03	0.34	0.02	0.33	0.02	0.35	0.02	0.33	0.03	0.32	0.08
Cu	0.38	0.04	0.36	0.06	0.34	0.03	0.34	0.04	0.32	0.03	0.27	0.04
Total	98.92		99.24		99.59		99.46		98.61		101.21	
Run No.	KK16-3		Cu10-2		Cu11-2		Cu11-3		Cu11-5			
n	32	σ	31	σ	54	σ	38	σ	25	σ		
O	0.49	0.21	6.32	1.06	0.53	0.30	0.50	0.33	1.09	0.34		
S	36.37	0.42	29.77	1.20	36.31	0.54	36.61	0.49	36.44	0.48		
Fe	61.22	0.44	60.76	2.38	58.29	1.20	57.21	0.91	57.48	0.80		
Ni	0.18	0.03	0.55	0.22	0.29	0.02	0.31	0.02	0.25	0.02		
Cu	0.28	0.03	3.59	2.03	4.09	1.15	4.51	0.79	4.18	0.74		
Total	98.54		100.99		99.51		99.14		99.43			

n.m. - not measured.
b.d.l. – below detection limit.

(Fig. 1b). Shimazaki and Maclean (1976) observed similar effects on the sulphide–silicate partitioning of Zn and Pb. They report a strong effect of oxygen content of sulphide on D_{Zn} and a similar, but weaker effect on D_{Pb}. Fonseca et al. (2011) have also observed a decrease in solubility of PGE in sulphide matte with increasing oxygen content of sulphide.

We considered possible ways to parameterise the dependence of $D_M^{sulph/sil}$ on the oxygen content of sulphide. We sought a simple model with the minimum number of adjustable parameters in which each of these parameters has some chemical meaning. Although mainly used for metal–silicate partitioning (Wade and Wood, 2005; Corgne et al., 2008; Tuff et al., 2011; Wood et al., 2014) and not developed for sulphides, we found that the ε-model of non-ideal interactions in metallic liquids (Wagner, 1962) meets these requirements and can, in most cases, reproduce trace element partitioning with a single "oxygen" parameter.

Taking the epsilon model (Ma, 2001) and simplifying for the case of highly dilute trace element M yields, for $MS_{n/2}$ dissolved in an FeS–FeO–NiS–$CuS_{0.5}$ matrix:

$$\log \gamma_{MS_{n/2}} = \log \gamma^0_{MS_{n/2}} + \log \gamma_{FeS} - \varepsilon^{FeO}_{MS_{n/2}} \log(1 - x_{FeO}) - \varepsilon^{NiS}_{MS_{n/2}} \log(1 - x_{NiS}) - \varepsilon^{CuS_{0.5}}_{MS_{n/2}} \log(1 - x_{CuS_{0.5}}) \quad (7)$$

In Eq. (7) γ_{FeS} and $\gamma_{MS_{n/2}}$ are, respectively the activity coefficients of FeS and $MS_{n/2}$ components in the sulphide, $\gamma^0_{MS_{n/2}}$ is the activity coefficient of $MS_{n/2}$ component at infinite dilution in FeS, x_i is the mole fraction of component i and ε^i_j is the interaction parameter between components i and j.

Although there are no data for the activity of FeS in the FeS–FeO–NiS–$CuS_{0.5}$ quaternary, a few simplifications and inferences may be made from considering the binary joins. The FeS–FeO binary exhibits a small negative deviation from ideality (Nagamori and Yazawa, 2001), while the FeS–NiS join shows small positive deviations from ideal behaviour (Fleet, 1989). Although the liquid join Cu_2S–FeS shows appreciable negative deviations from ideality (Eric and Timucin, 1981), we find that when the data of Eric and Timucin are recast as compositions on the join $CuS_{0.5}$–FeS the activity coefficients are much closer to 1. Given these observations we made the initial assumption that the activity coefficient of FeS in our experiments is approximately 1.0.

Assuming that FeS–FeO–NiS–$CuS_{0.5}$ solutions are in the Raoult's law region for FeS, the FeO content of the silicate melt employed in Eq. (4) is corrected for the mole fraction of FeS in the sulphide as follows (Kiseeva and Wood, 2013):

$$[FeO]_{corrected} = \frac{[FeO]_{silicate}}{[Fe/(Fe + Ni + Cu)]_{sulph}} \quad (8)$$

Table 4
Partition coefficients between sulphide and silicate liquids.

	Cu1-1	Cu2-1	Cu3-1	Cu4-1	Cu5-1	Cu6-1	Cu7-1	Cu8-1
Cu	399(24)	398(24)	454(54)	569(27)	620(58)	519(111)	653(145)	608(57)
Ga	0.07(1)	0.05(1)	0.05(1)	0.09(1)	0.10(1)	0.08(1)	0.09(2)	0.08(1)
Ge	1.25(12)	0.69(12)	0.77(7)	1.61(13)	1.93(11)	1.34(18)	1.62(16)	0.95(11)
Ag	364(63)	357(63)	395(41)	465(38)	507(67)	438(116)	507(106)	470(65)
Sb	21.6(1.2)	13.9(1.2)	15.0(1.3)	31.4(2.5)	36.9(3.6)	28.3(3.1)	30.2(3.4)	21.4(1.4)
Ti	0.0163(12)	0.0147(12)	0.0119(9)	0.0158(28)	0.0155(12)	0.0136(22)	0.0094(16)	0.0145(25)
V	0.34(2)	0.26(2)	0.25(1)	0.48(2)	0.52(3)	0.42(4)	0.44(8)	0.45(3)
Mn	0.59(3)	0.52(3)	0.46(2)	0.73(4)	0.86(4)	0.72(7)	0.89(14)	0.71(4)
Co	34(2)	30(2)	29(1)	56(3)	65(4)	48(4)	52(6)	55(4)
Zn	2.1(2)	1.6(2)	1.7(1)	2.7(2)	3.4(3)	3.0(4)	3.3(3)	2.5(2)
Cd	45(4)	37(4)	43(3)	70(7)	88(12)	67(10)	88(10)	61(6)
In	13.8(8)	9.6(8)	9.2(5)	17.9(9)	21.6(1.4)	18.1(2.1)	20.5(3.0)	14.8(1.0)
Tl	7.2(5)	6.8(5)	6.9(6)	8.2(8)	9.3(7)	9.0(1.1)	9.3(9)	8.1(7)
Pb	24(2)	21(2)	21(1)	34(2)	42(3)	35(4)	38(5)	33(3)
Cr	1.48(6)	1.17(6)	1.15(5)	2.31(13)	2.68(20)	2.12(22)	2.54(21)	2.36(13)
Ni	533(42)	433(42)	470(74)	843(108)	348(118)	549(156)	549(177)	833(140)
	Cu8-2	Cu9-1	Cu10-1	Cu11-1	Cu12-1	KK12-2	Ni3-1	Ni5-2
Cu	710(68)	724(45)	153(9)	729(145)	119(33)	61(19)	452(74)	316(28)
Ga	0.13(2)	0.09(1)	0.05(1)	0.25(3)	0.049(2)	0.10(1)	0.029(4)	0.02(1)
Ge	2.38(25)	1.08(8)	0.49(7)	3.94(41)	0.24(2)	0.41(4)	1.04(8)	1.24(7)
Ag	537(59)	557(35)	186(15)	843(155)	167(50)	88(29)	660(153)	369(83)
Sb	37.1(4.4)	23.9(1.7)	7.0(5)	95.2(8.8)	8.1(6)	4.0(4)	84.3(12.1)	70.8(4.9)
Ti	0.0124(24)	0.0099(17)	0.0443(62)	0.0539(96)	0.0408(27)	0.1505(61)	0.0354(44)	0.0019(16)
V	0.58(4)	0.44(1)	0.35(5)	1.04(9)	0.29(1)	0.63(2)	0.17(2)	0.04(1)
Mn	0.90(6)	0.89(4)	0.38(3)	1.94(11)	0.34(1)	0.47(1)	0.41(2)	0.12(1)
Co	65(4)	59(4)	16(1)	164(20)	16(1)	9(1)	71(3)	16(1)
Zn	3.8(2)	3.1(3)	1.1(1)	7.4(6)	0.7(1)	0.8(1)	1.5(1)	0.7(1)
Cd	85(9)	73(8)	25(2)	201(26)	15(2)	12(3)	51(8)	24(3)
In	23.5(1.7)	17.0(1.2)	4.9(3)	56.5(2.8)	3.7(2)	2.7(4)	16.7(1.8)	9.3(7)
Tl	10.1(8)	8.7(7)	5.8(3)	33.3(2.2)	5.1(4)	4.3(9)	13.2(2)	3.6(2)
Pb	43(3)	36(2)	11(1)	145(10)	9(1)	7(1)	51(8)	13(1)
Cr	2.88(25)	2.70(14)	0.87(10)	6.04(75)	0.78(4)	1.00(4)	1.33(23)	0.37(9)
Ni	1034(135)	931(81)	269(25)	1336(582)	292(84)	127(31)	1078(184)	305(20)
	Ni6-2	Ni7-1	KK4-6	KK4-7	KK4-8	KK4-9	KK4-10	KK15-6
Cu	494(121)	267(41)	224(21)	200(17)	566(58)	278(24)	592(60)	88(9)
Ga	0.05(1)	0.02(1)	0.25(6)	0.32(5)	0.053(4)	0.13(2)	0.043(2)	0.08(2)
Ge	1.43(25)	0.81(10)	4.16(78)	4.69(62)	0.73(6)	2.30(16)	0.53(4)	0.84(10)
Ag	436(54)	273(46)	234(21)	238(29)	633(34)	358(39)	649(49)	121(19)
Sb	54.1(5.7)	44.6(6.9)	50.2(6.1)	49.5(4.3)	18.6(8)	30.9(2.3)	15.4(9)	11.7(8)
Ti	0.0035(11)	0.0068(33)	0.0279(71)	0.0354(68)	0.0136(36)	0.0153(14)	0.0111(11)	0.0537(78)
V	0.32(4)	0.09(5)	0.98(7)	1.06(7)	0.33(2)	0.59(3)	0.36(2)	0.43(5)
Mn	0.37(2)	0.13(1)	1.01(4)	1.10(5)	0.53(1)	0.70(2)	0.53(1)	0.40(2)
Co	67(3)	32(1)	55(2)	52(3)	54(2)	46(1)	55(1)	13.8(4)
Zn	1.5(1)	0.6(1)	3.3(3)	3.4(2)	1.9(1)	2.7(2)	1.8(1)	1.1(1)
Cd	39(4)	20(5)	53(9)	49(4)	55(3)	56(5)	54(5)	19(2)
In	12.8(1.4)	6.9(1)	20.8(1.2)	22.0(1.6)	11.5(6)	17.6(1.8)	11.2(6)	5.8(4)
Tl	4.4(5)	3.2(6)	7.7(7)	9.6(1.0)	6.8(3)	8.9(1.2)	6.3(6)	4.7(5)
Pb	25(3)	13(3)	28(2)	31(3)	32(1)	32(4)	31(2)	10(1)
Cr	2.13(21)	0.64(44)	3.65(20)	3.86(22)	1.22(18)	2.59(10)	1.84(7)	1.03(10)
Ni	1162(65)	631(66)	567(84)	506(52)	1252(168)	633(63)	1264(167)	207(33)
	KK16-3	Cu10-2	Cu11-2	Cu11-3	Cu11-5			
Cu	292(42)	150(42)	374(66)	343(38)	523(82)			
Ga	0.95(12)	0.09(1)	0.58(14)	0.96(12)	0.23(3)			
Ge	12.2(1.5)	0.90(10)	9.1(1.3)	11.4(1.8)	3.80(64)			
Ag	388(51)	173(49)	467(82)	370(43)	616(121)			
Sb	195(12)	9.3(1.1)	157(18)	146(16)	81(9)			
Ti	0.0601(149)	0.0594(86)	0.0164(43)	0.0556(229)	0.0217(28)			
V	2.27(19)	0.43(7)	1.89(13)	2.13(11)	1.02(6)			
Mn	2.41(17)	0.40(2)	2.45(15)	2.64(8)	1.71(4)			
Co	129(11)	15(1)	131(11)	114(6)	116(6)			
Zn	7.9(7)	1.1(1)	8.1(1.3)	9.5(8)	6.3(4)			
Cd	125(22)	22(3)	143(32)	146(22)	141(19)			
In	54.2(3.2)	5.5(6)	66(11)	57(5)	43(4)			
Tl	23.2(1.5)	5.0(6)	32.3(5.3)	32(4)	30(4)			
Pb	94(7)	9(1)	122(21)	105(12)	104(12)			
Cr	8.31(68)	1.08(18)	7.96(60)	8.77(54)	5.67(27)			
Ni	909(173)	281(80)	911(185)	962(207)	1002(267)			

Strictly speaking, we should also correct the FeO content by dividing by the sulphur content of the sulphide as S/(S+O) i.e. make an entropic correction for S–O mixing in sulphide. However, this correction makes the algebra more complex, so we omit it here, but give an extended description including this term in Supplementary Information. Adding the activity coefficient for $MS_{n/2}$ dissolved in the sulphide (Eq. (7)) and assuming that all terms are adequately accounted for, we obtain:

$$\log D_M^{sulph/sil} = A - \frac{n}{2}\log[\mathrm{FeO}]_{corr} + \varepsilon^{\mathrm{FeO}}_{\mathrm{MS}_{n/2}}\log(1-x_{\mathrm{FeO}}) + \varepsilon^{\mathrm{NiS}}_{\mathrm{MS}_{n/2}}\log(1-x_{\mathrm{NiS}}) + \varepsilon^{\mathrm{CuS_{0.5}}}_{\mathrm{MS}_{n/2}}\log(1-x_{\mathrm{CuS_{0.5}}}) \quad (9)$$

We fitted our data to Eq. (9) on an element by element basis using the stepwise linear regression model of the SPSS statistical package. This generated the fitted lines shown in Figs. 2 and 3 and fit parameters given in Table 5. To test the sensitivity of the regression model, we broke the procedure into two independent steps. We first calculated $\varepsilon^{\mathrm{FeO}}$ incorporating only the experiments with low Ni and Cu contents (below 10 wt% (Ni + Cu) in sulphide liquid). Then, we corrected the entire dataset for the oxygen-term and used a stepwise linear regression model to generate $\varepsilon^{\mathrm{NiS}}$ and $\varepsilon^{\mathrm{CuS_{0.5}}}$. For both approaches the epsilon-values were within uncertainty (Table 5). Note that by omitting the entropy of S–O mixing we have "buried" this term in the $\varepsilon^{\mathrm{FeO}}$ term.

To show how the model can be applied to our partitioning data, we selected one element (Ga) and applied the corrections sequentially in order to illustrate the effect of each parameter. The results are shown in Supplementary Fig. 4. The same procedure was then applied to every element plotted in Figs. 2 and 3.

3.2. Effect of temperature

Having obtained Eq. (9) which relates the partition coefficient of element M to the FeO content of the silicate melt and the NiS, $CuS_{0.5}$ and FeO contents of the sulphide melt, the next question is that of temperature. We constrained temperature effects on partitioning of our 16 elements by performing experiments over a temperature range of 1300 to 1700 °C (Table 1). These experiments together with 1400 °C data from the experiments with the same silicate compositions in our previous and current studies were used to determine the temperature-effects on element partitioning.

We model the effect of temperature by adding an enthalpy term to Eq. (9) and taking account of the temperature dependence of epsilon by scaling with temperature:

$$\log D_M^{sulph/sil} = A + \frac{B}{T} - \frac{n}{2}\log[\mathrm{FeO}]_{corr} + \frac{1673}{T}\left[\varepsilon^{\mathrm{FeO}}_{\mathrm{MS}_{n/2}}\log(1-x_{\mathrm{FeO}}) + \varepsilon^{\mathrm{NiS}}_{\mathrm{MS}_{n/2}}\log(1-x_{\mathrm{NiS}}) + \varepsilon^{\mathrm{CuS_{0.5}}}_{\mathrm{MS}_{n/2}}\log(1-x_{\mathrm{CuS_{0.5}}})\right] \quad (10)$$

We fitted for B by linear regression with the results given in Table 5 and illustrated in Fig. 4. In our previous study, we used the thermodynamic data of Barin et al. (1989) to decompose the constant term into temperature-dependent and temperature-independent terms for Cu, Zn, Pb and Mn (Kiseeva and Wood, 2013). The measured temperature effects for Mn and Pb are almost identical to those predicted, while for Cu and Zn the temperature effects are more negative than those derived from thermodynamic data. The results (Table 5) indicate small or zero temperature effects on partitioning of Co, Cd, In, Mn, Pb, Tl and Zn. Strong negative T-dependences are observed for the more chalcophile elements Ag, Ni and Cu. Lithophile elements Ga, Ge, Cr, V and Ti have positive dependences of D on temperature.

To simplify usage of Eq. (10) we have created an Excel spreadsheet "D calculator" which is attached as Supplementary Material to this paper.

4. Discussion

4.1. Sulphide precipitation and sulphur solubility

It has been widely acknowledged in the literature that sulphur solubility in silicate magmas plays an important role in controlling concentrations of highly chalcophile elements, such as the PGEs, Cu and Ag (e.g. Lee et al., 2012; Li, 2014) during magma genesis and differentiation. Recognition of this importance has led to development of a number of models of S solubility in silicate melts (Holzheid and Grove, 2002; Li and Ripley, 2009; Liu et al., 2007; Mavrogenes and O'Neill, 1999; O'Neill and Mavrogenes, 2002). Although the models generally agree that the FeO contents of silicate liquids, pressure and temperature are dominant controls on SCSS (sulphur content at sulphide saturation), they diverge widely in their predictions of S solubility in, for example, differentiating basaltic magmas. For instance, according to Mavrogenes and O'Neill (1999), at low pressures about 60% crystallisation is required for basaltic liquids to achieve sulphur saturation, while Li and Ripley (2005) estimate about 10% fractional crystallisation for a MORB-liquid to reach sulphide saturation.

We are able to test these different solubility models using our sulphide–silicate partitioning data, which we have applied to a set of MORB glasses (Jenner and O'Neill, 2012). Cu and Ag are incompatible in silicate phases but they have high and virtually identical partition coefficients into sulphides. Their similar geochemical behaviour during mantle melting is manifested by a nearly constant Cu/Ag ratio of 3500 ± 500 along the liquid line of MORB descent (Jenner and O'Neill, 2012).

If we begin with an initial concentration S_0 of sulphur in a melt and allow $X_{sulphide}$ (fraction of sulphide) to precipitate at saturation then we have:

$$\mathrm{SCSS} = \frac{S_0 - X_{sulphide}S_{sulphide}}{X_{melt}} \quad (11)$$

where X_{melt} is fraction of silicate melt left and $S_{sulphide}$ is the concentration of sulphur in sulphide. According to Jenner and O'Neill (2012), the initial amount of sulphur (S_0) in MORB magmas at ≥9 wt% MgO is around 900–1000 ppm. The fraction of residual silicate melt, X_{melt}, remaining during fractional crystallisation of MORB was parameterised as a function of the MgO content of the liquid using Petrolog3 (Danyushevsky and Plechov, 2011). We began with a MORB liquid containing 9.3% MgO (from Jenner and O'Neill, 2012) and fractionally crystallised it. The input parameters were constant pressure at 3 kbar and temperature on the olivine liquidus. The Petrolog3 software generated the following crystallisation sequence: olivine, plagioclase, clinopyroxene, spinel and orthopyroxene. The modelling was stopped at 5.8 wt% MgO at which point 33% melt remained. $X_{sulphide}$ was calculated using the equilibrium crystallisation equation to estimate the amount of sulphide precipitated along the liquid line of descent from our values of D_{Cu} and Jenner and O'Neill's (2012) analyses of MORB glasses.

$$X_{sulphide} = \frac{\frac{C_0^{\mathrm{Cu}}}{C_i^{\mathrm{Cu}}} - F}{D_{\mathrm{Cu}}} \quad (12)$$

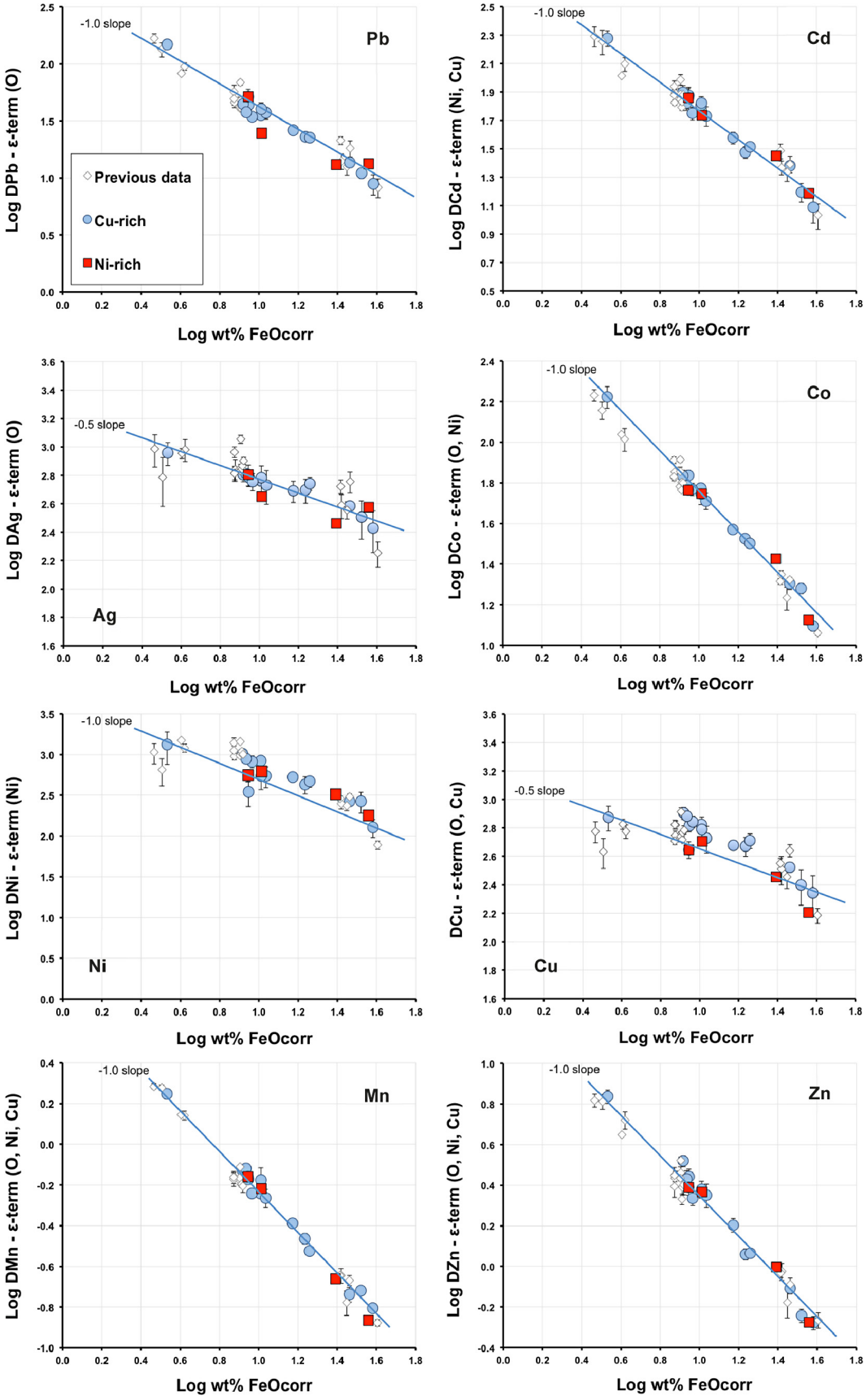

Fig. 2. Corrected Log $D^{(sulphide-silicate)}$ values plotted versus corrected log[FeO] content (wt%) of the silicate melt. Partitioning data from Tables 2 and 5, and from Kiseeva and Wood (2013). Error bars (shown where larger than symbols) were calculated, using error propagation, from the standard deviations in Supplementary Tables 1 and 2. All the experiments were performed with either MORB or CMAS silicate melt composition (see Table 1). All of the experimental data were used for the fit to Eq. (9). The fit parameters and uncertainties are presented in Table 5.

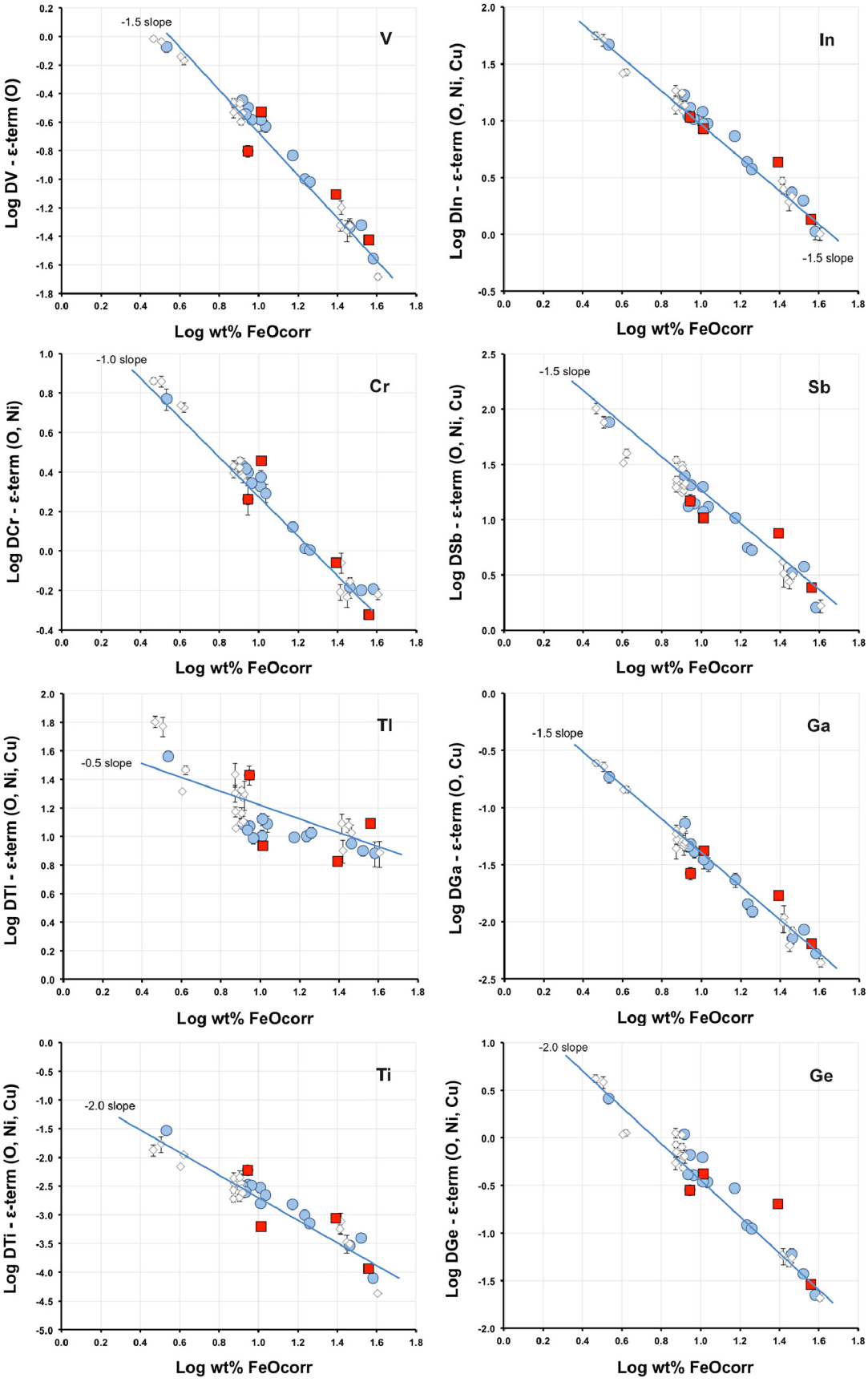

Fig. 3. Corrected Log $D^{(sulphide-silicate)}$ values plotted versus corrected log[FeO] content (wt%) of the silicate melt. Partitioning data from Tables 2 and 5, and from Kiseeva and Wood (2013). Error bars (shown where larger than symbols) were calculated, using error propagation, from the standard deviations in Supplementary Tables 1 and 2. All the experiments were performed with either MORB or CMAS silicate melt composition (see Table 1). All of the experimental data were used for the fit to Eq. (9). The fit parameters and uncertainties are presented in Table 5. Symbols as in Fig. 2.

Table 5
Equation parameters for the partition coefficients between sulphide and silicate liquids.

Element	ε_{FeO}	σ	ε_{NiS}	σ	$\varepsilon_{CuS_{0.5}}$	σ	A	σ	B	σ
Cu	2.20	0.29	insign	–	−1.03	0.36	0.700	0.328	4200	570
Ni	insign	–	−0.90	0.30	insign	–	1.869	0.483	3300	840
Pb	0.45	0.18	insign	–	insign	–	1.834	0.278	1260	480
Ag	1.90	0.23	insign	–	insign	–	0.724	0.311	4300	540
Zn	−0.67	0.13	0.69	0.10	−1.02	0.16	1.915	0.129	−990	230
Cd	insign	–	0.48	0.12	−1.06	0.20	1.919	0.214	1420	370
Tl	0.99	0.40	0.95	0.30	0.98	0.47	1.678	0.045	insign	–
Mn	−1.90	0.10	0.76	0.08	−0.41	0.12	1.629	0.147	−1520	260
In	−1.61	0.22	−0.54	0.16	−2.36	0.26	2.502	0.024	insign	–
Ti	−12.91	0.59	−2.22	0.44	−2.04	0.70	1.027	0.663	−2740	1150
Ga	−5.09	0.21	insign	–	−1.89	0.26	3.347	0.288	−5470	500
Sb	−1.52	0.30	−2.32	0.23	−2.95	0.35	4.303	0.250	−2670	440
Co	0.60	0.13	−0.28	0.10	insign	–	1.964	0.127	1280	220
V	−5.34	0.21	insign	–	insign	–	2.524	0.239	−2840	420
Ge	−4.94	0.43	−1.65	0.32	−4.07	0.51	4.635	0.450	−5000	780
Cr	−0.76	0.14	0.44	0.11	insign	–	2.356	0.190	−1810	330
Element	ε'_{FeO}	σ	ε'_{NiS}	σ	$\varepsilon'_{CuS_{0.5}}$	σ				
Cu	2.37	0.34	insign	–	−1.72	0.63				
Ni	insign	–	−0.83	0.30	insign	–				
Pb	0.54	0.20	insign	–	insign	–				
Ag	1.99	0.29	insign	–	insign	–				
Zn	−0.70	0.16	0.68	0.09	−1.03	0.15				
Cd	insign	–	0.53	0.12	−1.03	0.19				
Tl	1.02	0.43	0.95	0.28	0.99	0.46				
Mn	−1.98	0.11	0.74	0.07	−0.42	0.12				
In	−1.39	0.21	−0.49	0.15	−2.33	0.25				
Ti	−12.64	0.58	−2.15	0.41	−2.00	0.68				
Ga	−5.04	0.20	insign	–	−1.88	0.25				
Sb	−1.12	0.26	−2.22	0.21	−2.89	0.35				
Co	0.66	0.12	−0.27	0.09	insign	–				
V	−5.40	0.20	insign	–	insign	–				
Ge	−4.47	0.34	−1.53	0.31	−3.99	0.51				
Cr	−0.82	0.12	0.42	0.10	insign	–				

Insign – insignificant.
ε, A and B are the regression parameters for the linear equation:
$\text{Log}\, D = A + \frac{B}{T} - \frac{n}{2}\log(\text{FeO})_{corr} + \frac{1673}{T}\varepsilon^{\text{FeO}}\log(1 - X_{\text{FeO}}^{sulph}) + \frac{1673}{T}\varepsilon^{\text{NiS}}\log(1 - X_{\text{NiS}}^{sulph}) + \frac{1673}{T}\varepsilon^{\text{CuS}_{0.5}}\log(1 - X_{\text{CuS}_{0.5}}^{sulph})$.
ε(FeO), ε(NiS) and $\varepsilon(\text{CuS}_{0.5})$ are calculated using multiple regression for all three independent parameters (FeO, $\text{CuS}_{0.5}$ and NiS) simultaneously with all the experimental dataset included into calculations.
ε'(FeO) is calculated based only on Ni- and Cu-poor experiments (below 10% admixture of Ni and Cu together). Then, the correction for FeO in sulphide is applied and the entire set of experimental data is regressed to determine interaction parameters for NiS and $\text{CuS}_{0.5}$.
T-term was introduced after the epsilon-correction was done.
FeO is corrected according to Eq. (8).

where F is X_{melt}, C_i^{Cu} is the concentration of Cu in the liquid, C_0^{Cu} is initial concentration of Cu in the liquid and D_{Cu} is the sulphide–silicate partition coefficient of Cu. Given that

$$F = 1 - X_{sulphide} - X_{crystals} \tag{13}$$

where $X_{crystals}$ is fraction of crystals and that $X_{sulphide}$ is very small, we can approximate:

$$F = 1 - X_{crystals} \tag{14}$$

and solve Eq. (12) directly for $X_{sulphide}$. The initial Cu content C_0^{Cu} of about 100 ppm was taken from Jenner and O'Neill (2012) at ≥9 wt% MgO. D_{Cu} was calculated using Eq. (10), but since the amount of Cu and FeO in MORB magmas along the liquid line of descent is not constant, we also needed to estimate the evolution of sulphide composition. According to our model the sulphide composition varies between almost 25 wt% Ni and 8 wt% Cu for primitive MORB (9.3 wt% MgO) and 6 wt% Ni, 5.5 wt% Cu for evolved MORB (6 wt% MgO). Temperatures were taken from our modelling using Petrolog3 and varied from 1230 to 1175 °C during crystallisation. Average D_{Cu} in this interval is about 850. The concentration of sulphur in sulphide, $S_{sulphide}$ averages 33 wt%. We used the equilibrium crystallisation model rather than Rayleigh fractionation because Rehkämper et al. (1999) showed that the former describes the behaviour of platinum group elements, which partition strongly into sulphide, better than Rayleigh fractionation.

The calculated fraction of precipitated sulphide along the liquid line of descent, assuming equilibrium segregation, reaches only 0.23% at about 6 wt% MgO in silicate melt (Fig. 5a). If we had used the Rayleigh fractionation equation the amount of precipitated sulphide would be less, about 0.14%. According to either set of assumptions however, most of the silicate melt compositions reported by Jenner and O'Neill (2012) should have precipitated sulphide.

Calculated values of SCSS for the entire Jenner and O'Neill (2012) glass dataset are plotted in Fig. 5b. For comparison, we added SCSS calculated for the same P–T conditions by other models in the literature. As can be seen the trend and scatter of our calculated SCSS values are in very good agreement with Jenner and O'Neill's S-content measurements. Of the experimentally-based models in the literature our values are in best agreement with the SCSS models of Liu et al. (2007) and Li and Ripley (2009) (Fig. 5b).

4.2. Pb content of depleted mantle

Because Ce and Nd are more compatible in mantle silicates (principally clinopyroxene) than Pb (Hart and Dunn, 1993; Wood and Blundy, 1997; Klemme et al., 2002), nearly constant Ce/Pb ~25 and Nd/Pb ~20 ratios observed in MORB and OIB magmas have been attributed to retention of Pb by residual sulphide (Hart and Gaetani, 2006). The observed near-constancy of these ratios enable us to estimate the Pb content of depleted mantle.

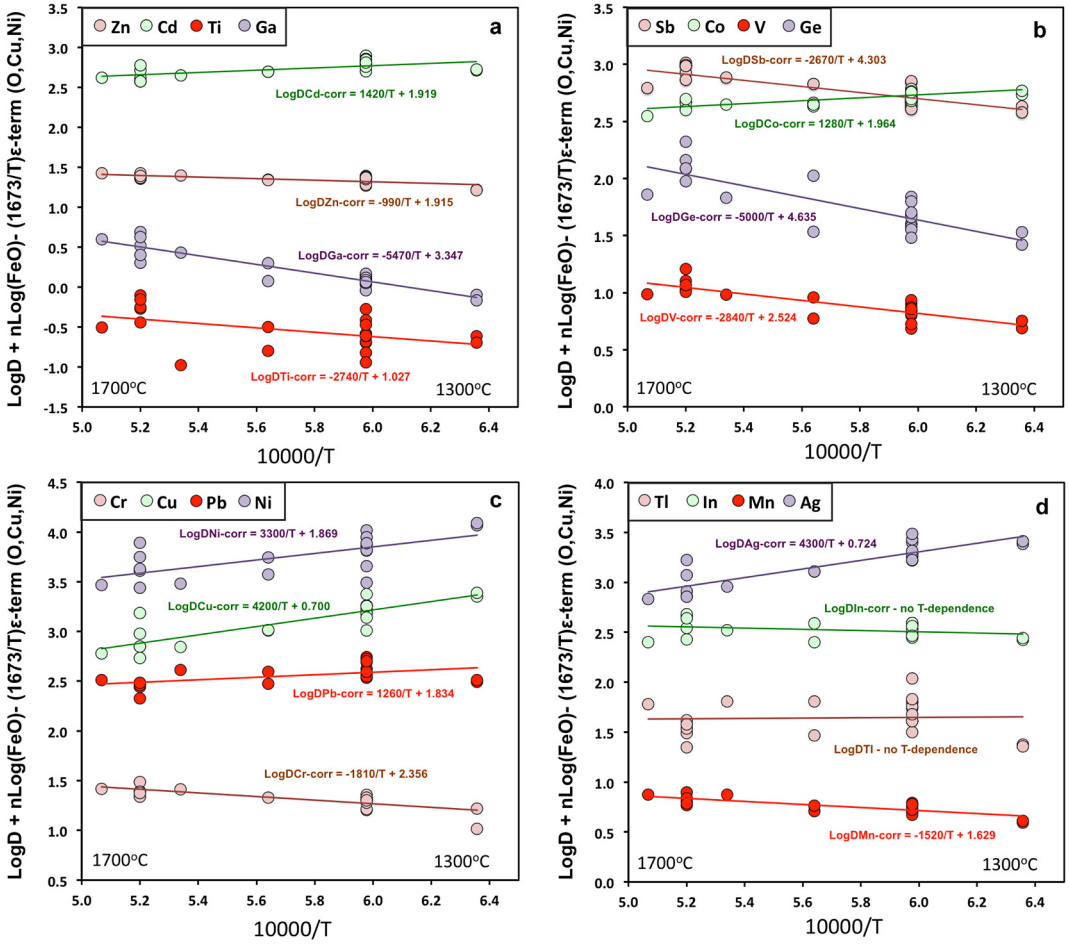

Fig. 4. The effect of temperature on sulphide–silicate partitioning as modelled using Eq. (10). Fit parameters are presented in Table 5.

Workman and Hart (2005) and Salters and Stracke (2004) made similar estimates of the Ce and Nd contents of depleted mantle of 550 and 772 ppb and 581 and 713 ppb, respectively. Values in these ranges reproduce the ~5.9 ppm Ce and ~5.2 ppm Nd observed in primitive MORB glasses (>9% MgO) by Jenner and O'Neill (2012) given 10% mantle melting at 1.5 GPa (Robinson et al., 1998) and D_{Ce} and D_{Nd} into clinopyroxene of 0.12 and 0.25, respectively (Wood and Blundy, 1997). We calculated the major element composition of mantle sulphide in equilibrium with such MORB liquids from the ~200 ppm Ni and ~100 ppm Cu reported by Jenner and O'Neill (2012) in primitive MORB glasses (with ≥9 wt% MgO). Assuming $T = 1230\,^{\circ}C$ and FeO = 9 wt% in silicate liquid, we obtain sulphide that contains 22 wt% Ni, 8 wt% Cu, 1 wt% O and 36.5 wt% Fe to be in equilibrium with the most primitive MORB liquids and a D_{Pb} value of 29.

In order to achieve Ce/Pb of about 25 and Nd/Pb of about 20 at 10% melting of a depleted mantle containing 100 ppm S, initial concentrations are Ce ~650 ppm, Nd ~550 ppm and Pb ~25 ppb. These are consistent with estimates by Salters and Stracke (2004), who reported 772 ppm of Ce, 713 ppm of Nd and 23.2 ppb of Pb in the depleted mantle. If we increase the S content of the mantle to 300 ppm we only increase the Pb value to 30 ppb. For these calculations we assumed constant S-solubility of about 900 ppm. An increase in S-solubility from 900 to 1200 ppm (estimated by Fortin et al., 2015, for primitive MORB) decreases the estimated Pb content of the depleted mantle by less than 0.5 ppb.

4.3. Hadean matte

It is instructive to consider partitioning of the elements of interest into the putative sulphide matte, which has been proposed (O'Neill, 1991) as having established the concentrations of chalcophile elements in the silicate Earth in the later stages of accretion. Conventionally, abundances are plotted as a function of temperature at which 50% of the element would condense from a gas of solar composition (T_{50}) in order to emphasise the trend of decreasing abundance with increasing volatility. This type of plot (Wood et al., 2010) shows some anomalies, which are difficult to explain. Indium, for example, appears to be overabundant for an element of its volatility, while Cu and Ag are remarkably different in abundance despite being of almost identical condensation temperature and very similar partitioning behaviour into both sulphides and metals (Wood et al., 2014). One of the problems, of course, is that some of the data required to make the calculations are sparse and approximations need to be made. We therefore repeated the condensation calculations for the elements Cu, Ag, Pb and Zn to investigate the nature of the approximations and sources of uncertainties. Our calculations are based on solar system abundances from Lodders (2003) and a major element condensation sequence at 10^{-4} bar computed using previously published software (Wood and Hashimoto, 1993). Condensation of 50% of the element of interest into the appropriate phase was then calculated from thermodynamic data (Barin et al., 1989) for gas and solid species which, since the solids used are simple metals and sulphides, was performed in a spreadsheet. Supplementary Table 4 shows a comparison of 50% condensation temperatures from different sources,

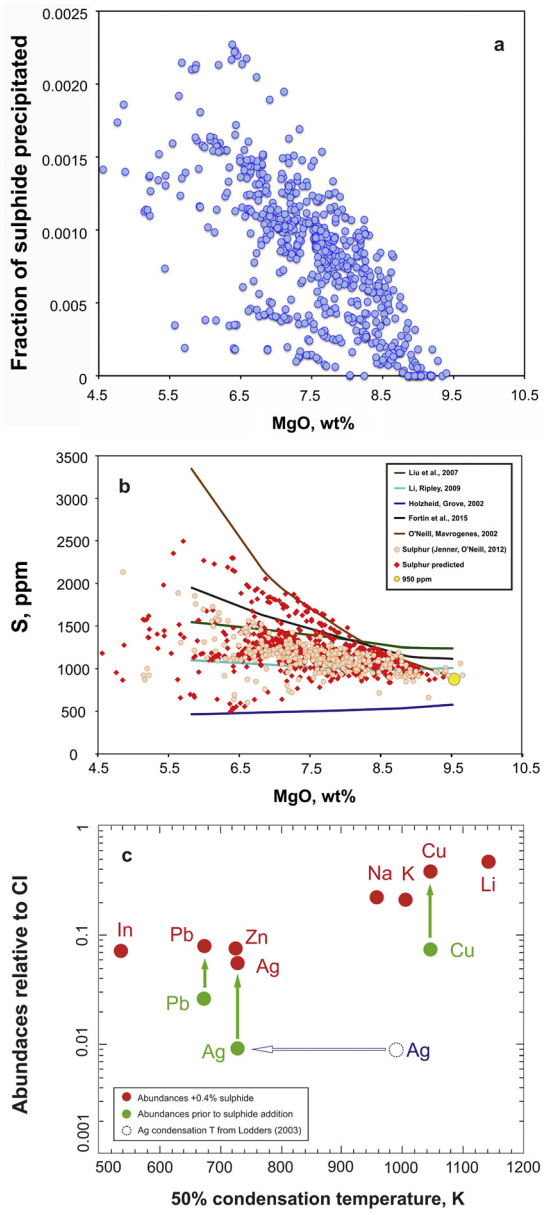

Fig. 5. (a) Calculated fraction of sulphide precipitated from MORB liquids along the liquid line of descent. Cu contents of MORB glasses (Jenner and O'Neill, 2012) were used as the basis of the calculation (see text). (b) Sulphur contents of MORB glasses at sulphide saturation [SCSS] derived from data of (a). (c) Abundances of elements in the bulk silicate earth relative to CI chondrites plotted as a function of 50% condensation temperature from a gas of solar composition. Note the revised condensation temperature of Ag (see text) and the effects of "adding-back" 0.4% sulphide matte to the mantle.

together with our calculations. The calculated 50% condensation temperature of Cu is 1178 K at a total pressure of 10^{-4} bar if ideal solution in solid Fe metal is assumed. An earlier study (Wai and Wasson, 1977) obtained 1170 K making the same assumption. In contrast, Lodders (2003) gives a 50% condensation temperature of 1037 K into Fe metal without giving detailed information on the nature of the Fe–Cu solid solution. However, we find that we are able to closely reproduce the author's result obtaining 1047 K if we take account of the very low solubility of Cu in alpha-Fe at 1133 K (Chen and Jin, 1995) and extrapolate the derived activity coefficient of 52 down temperature by assuming that RTlogγ is a constant. For Ag, Lodders (2003) obtained a 50% condensation temperature at 10^{-4} bar of 996 K with this element entering Fe metal in the condensation sequence. Calculations by ourselves and Wai and Wasson (1977) give virtually identical values to those of Lodders provided Ag is assumed to dissolve ideally in alpha-Fe. In fact, Ag is much less soluble than Cu in iron which means that the activity coefficients are even higher than those for Cu. The measured solubility of Ag in gamma-Fe at 1366 K leads to a maximum X_{Ag} of 3.7×10^{-5} (Wriedt et al., 1973) which means that the activity coefficient is about 27 000. Using this value and applying the same form of temperature dependence as for Cu, results in a condensation temperature into Fe of <600 K. However, the strongly chalcophile nature of Ag means that it would actually condense into FeS almost as soon as sulphide appears in the sequence at just over 700 K i.e. nearly 300 K below the tabulated condensation temperature. Assuming, by analogy with the FeS–$CuS_{0.5}$ system discussed earlier, ideal solution between FeS and $AgS_{0.5}$ leads to a 50% condensation temperature of 730 K (Fig. 5c). This result is, because of the highly chalcophile nature of Ag, relatively insensitive to nonideality in the sulphide.

A comparison between Pb and Zn, which are both 2+ ions of different degrees of chalcophile behaviour is also instructive. Lodders (2003) calculates a 50% condensation temperature of 727 K for Pb entering metallic Fe. We generate an almost identical value of 740 K if we assume that Pb dissolves ideally in Fe. However, the activity coefficient of Pb dissolved in solid Fe at 1000 K is about 5×10^4 (Vaajamo and Taskinen, 2011) and this leads to a condensation temperature for Pb into iron of <500 K. We find, instead that Pb should condense into sulphide soon after FeS appears. Assuming that FeS–PbS solid solutions are, like FeS–PbS liquids, close to ideal (Eric and Timucin, 1981) the 50% condensation temperature of Pb into sulphide is calculated to be 675 K. This result, about 50 K lower than Lodders' tabulated temperature, is likely to be an overestimate because of the ideality assumption. In contrast to Ag and Pb we find good agreement with previous results for Zn, obtaining a condensation temperature of 730 K, in good agreement with Lodders' 727 K.

Fig. 5c shows abundances of these chalcophile elements and some lithophile elements of similar volatility in silicate Earth as a function of 50% condensation temperature from a gas of solar composition at 10^{-4} bar. This figure shows the well-known correlation for lithophile elements between abundance and condensation temperature and demonstrates that the correlation for chalcophile elements Pb, Ag and Cu is improved by the revised temperatures discussed above. Then, to simulate the effects of removal of Hadean matte we have calculated the composition of sulphide in equilibrium with a silicate melt of mantle composition and added back different amounts of sulphide to see if the correlation between abundance and condensation temperature can be improved. The example shown, which is illustrative rather than definitive, is for addition of 0.4% sulphide to a mantle which is 98% crystals and 2% silicate melt. This shows that removal of a small amount of sulphide from a crystal-rich mush would disturb a "smooth" temperature-abundance pattern and create the pattern observed. The conclusion is that removal of a small amount of Hadean matte is a plausible explanation for the pattern of chalcophile element abundances in the mantle.

5. Conclusions

The partitioning of chalcophile elements between sulphide liquid and silicate melt can be represented either in terms of an equilibrium involving oxygen and sulphur or as an exchange reaction involving FeO in the silicate melt and FeS in the sulphide. The latter approach has, as shown in an earlier paper (Kiseeva and Wood, 2013), much greater geological utility in that partition coefficients D_i are proportional to the FeO content of the silicate melt to a negative power related to the valency of i, $(FeO)^{-n}$.

Our detailed study of the partitioning of Ag, Cd, Co, Cr, Cu, Ga, Ge, In, Mn, Ni, Pb, Sb, Ti, Tl, V and Zn between sulphide and silicate shows that the power of D_i dependence on FeO concentration in silicate deviates from the ideal value of −0.5 times valency because of increasing oxygen content of sulphide with increasing FeO in silicate. Oxyphile elements such as Mn follow O into sulphide, increasing this power while chalcophile elements such as Cu are repelled by oxygen which decreases the power of FeO dependence. This effect has been parameterised using the ε-model of non-ideal interactions in metallic liquids. For completeness, we applied this approach to sulphides in the system FeS–FeO–NiS–$CuS_{0.5}$ i.e. to sulphides containing substantial Ni and/or Cu in addition to O. We find that ε^{FeO}, which parameterises the effect of oxygen, represents the principal non-ideal effect for most elements while ε^{NiS} and $\varepsilon^{CuS_{0.5}}$ are usually much smaller.

After taking account of the effect of temperature on partition coefficients we have a partitioning model for the 16 elements of interest calibrated for the temperature range 1300–1700 °C and potentially applicable to temperatures several hundred degrees outside this range. When applied to the Cu and Ag contents of MORB's we are able to show that, during silicate crystallisation the glasses analysed by Jenner and O'Neill (2012) were saturated in sulphide, but that the total amount precipitated during 70% silicate crystallisation was only about 0.23%. The computed extents of sulphide precipitation enable us to calculate the sulphur concentrations at sulphide saturation (SCSS) for these melts with results which are in best agreement with the recently developed model of Fortin et al. (2015). We are also able to use the canonical Ce/Pb and Nd/Pb ratios of MORB of ∼25 and ∼20 respectively to calculate the Pb content of the depleted mantle. Given estimates of the Ce (650 ppb) and Nd (550 ppb) contents of the MORB source we obtain a Pb content of ∼27.5 ppb assuming sulphide saturation.

We made an illustrative calculation of the properties of the putative Hadean matte which, it has been suggested (e.g. O'Neill, 1991), was extracted from the mantle to the core thereby establishing the chalcophile element concentrations in bulk silicate earth. Treating Cu, Ag, Pb and Zn as examples, we added-back equilibrium sulphide to silicate Earth in order to establish a smooth pattern of elemental abundance as a function of 50% condensation temperature. We find that addition of 0.4% sulphide liquid to a mantle which was 98% crystals, 2% silicate melt would produce the anticipated pattern (Fig. 5c).

An MS Excel Spreadsheet, provided in Supplementary Information, enables use of our model to calculate the composition of sulphide in equilibrium with silicate liquid and the D-values for the 16 elements of interest given FeO, Ni and Cu contents of the silicate melt.

Acknowledgements

We acknowledge support from European Research Council grant 267764 to BJW and the NERC grant NE/L010828/1 to ESK. We also thank two anonymous reviewers for their constructive comments.

Appendix A. Supplementary material

Supplementary material related to this article can be found online at http://dx.doi.org/10.1016/j.epsl.2015.05.012.

References

Barin, I., Sauert, F., Schultze-Rhonhof, E., Sheng, W.S., 1989. Thermochemical Data of Pure Substances, Parts I and II. CH Verlagsgesellschaft, Weinheim, Germany.

Chen, Q., Jin, Z.P., 1995. The Fe–Cu system – a thermodynamic evaluation. Metall. Mater. Trans. A 26, 417–426.

Corgne, A., Keshav, S., Wood, B.J., McDonough, W.F., Fei, Y.W., 2008. Metal–silicate partitioning and constraints on core composition and oxygen fugacity during Earth accretion. Geochim. Cosmochim. Acta 72, 574–589.

Czamanske, G.K., Moore, J.G., 1977. Composition and phase chemistry of sulfide globules in basalt from Mid-Atlantic Ridge rift valley near 37°N lat. Geol. Soc. Am. Bull. 88, 587–599.

Danyushevsky, L.V., Plechov, P., 2011. Petrolog3: integrated software for modeling crystallization processes. Geochem. Geophys. Geosyst. 12, Q07021.

Dreibus, G., Palme, H., 1996. Cosmochemical constraints on the sulfur content in the Earth's core. Geochim. Cosmochim. Acta 60, 1125–1130.

Eric, H., Timucin, M., 1981. Activities in Cu_2S–FeS–PbS melts at 1200 °C. Metall. Trans. B 12, 493–500.

Falloon, T.J., Green, D.H., 1987. Anhydrous partial melting of MORB pyrolite and other peridotite compositions at 10 kbar – implications for the origin of primitive MORB glasses. Mineral. Petrol. 37, 181–219.

Fleet, M.E., 1989. Activity coefficients for FeS and NiS in monosulfide liquid and $NiSi_{1/2}O_2$ in olivine from sulfide–silicate equilibria. Geochim. Cosmochim. Acta 53, 791–796.

Fonseca, R.O.C., Campbell, I.H., O'Neill, H.S.C., Fitzgerald, J.D., 2008. Oxygen solubility and speciation in sulphide-rich mattes. Geochim. Cosmochim. Acta 72, 2619–2635.

Fonseca, R.O.C., Mallmann, G., O'Neill, H.S., Campbell, I.H., Laurenz, V., 2011. Solubility of Os and Ir in sulfide melt: implications for Re/Os fractionation during mantle melting. Earth Planet. Sci. Lett. 311, 339–350.

Fortin, M.-A., Riddle, J., Desjardins-Langlais, Y., Baker, D.R., 2015. The effect of water on the sulfur concentration at sulfide saturation (SCSS) in natural melts. Geochim. Cosmochim. Acta 160, 100–116. http://dx.doi.org/10.1016/j.gca.2015.03.022.

Gaetani, G.A., Grove, T.L., 1997. Partitioning of moderately siderophile elements among olivine, silicate melt, and sulfide melt: constraints on core formation in the Earth and Mars. Geochim. Cosmochim. Acta 61, 1829–1846.

Hart, S.R., Dunn, T., 1993. Experimental Cpx melt partitioning of 24 trace-elements. Contrib. Mineral. Petrol. 113, 1–8.

Hart, S.R., Gaetani, G.A., 2006. Mantle Pb paradoxes: the sulfide solution. Contrib. Mineral. Petrol. 152, 295–308.

Holzheid, A., Grove, T.L., 2002. Sulfur saturation limits in silicate melts and their implications for core formation scenarios for terrestrial planets. Am. Mineral. 87, 227–237.

Holzheid, A., Lodders, K., 2001. Solubility of copper in silicate melts as function of oxygen and sulfur fugacities, temperature, and silicate composition. Geochim. Cosmochim. Acta 65, 1933–1951.

Jenner, F.E., O'Neill, H.S., 2012. Major and trace analysis of basaltic glasses by laser-ablation ICP-MS. Geochem. Geophys. Geosyst. 13.

Kiseeva, E.S., Wood, B.J., 2013. A simple model for chalcophile element partitioning between sulphide and silicate liquids with geochemical applications. Earth Planet. Sci. Lett. 383, 68–81.

Klemme, S., Blundy, J.D., Wood, B.J., 2002. Experimental constraints on major and trace element partitioning during partial melting of eclogite. Geochim. Cosmochim. Acta 66, 3109–3123.

Kress, V., 2007. Thermochemistry of sulfide liquids III: Ni-bearing liquids at 1 bar. Contrib. Mineral. Petrol. 154, 191–204.

Lee, C.T.A., Luffi, P., Chin, E.J., Bouchet, R., Dasgupta, R., Morton, D.M., Le Roux, V., Yin, Q.Z., Jin, D., 2012. Copper systematics in arc magmas and implications for crust–mantle differentiation. Science 336, 64–68.

Li, C.S., Ripley, E.M., 2005. Empirical equations to predict the sulfur content of mafic magmas at sulfide saturation and applications to magmatic sulfide deposits. Miner. Depos. 40, 218–230.

Li, C.S., Ripley, E.M., 2009. Sulfur contents at sulfide-liquid or anhydrite saturation in silicate melts: empirical equations and example applications. Econ. Geol. 104, 405–412.

Li, J., Agee, C.B., 1996. Geochemistry of mantle–core differentiation at high pressure. Nature 381, 686–689.

Li, Y., 2014. Chalcophile element partitioning between sulfide phases and hydrous mantle melt: applications to mantle melting and the formation of ore deposits. J. Asian Earth Sci. 94, 77–93.

Li, Y., Audétat, A., 2012. Partitioning of V, Mn, Co, Ni, Cu, Zn, As, Mo, Ag, Sn, Sb, W, Au, Pb, and Bi between sulfide phases and hydrous basanite melt at upper mantle conditions. Earth Planet. Sci. Lett. 355–356, 327–340.

Liu, Y.N., Samaha, N.T., Baker, D.R., 2007. Sulfur concentration at sulfide saturation (SCSS) in magmatic silicate melts. Geochim. Cosmochim. Acta 71, 1783–1799.

Lodders, K., 2003. Solar system abundances and condensation temperatures of the elements. Astrophys. J. 591, 1220–1247.

Ma, Z.T., 2001. Thermodynamic description for concentrated metallic solutions using interaction parameters. Metall. Mater. Trans. B 32, 87–103.

Matzen, A.K., Baker, M.B., Beckett, J.R., Stolper, E.M., 2013. The temperature and pressure dependence of nickel partitioning between olivine and silicate melt. J. Petrol. 54, 2521–2545.

Mavrogenes, J.A., O'Neill, H.S.C., 1999. The relative effects of pressure, temperature and oxygen fugacity on the solubility of sulfide in mafic magmas. Geochim. Cosmochim. Acta 63, 1173–1180.

Mungall, J.E., Brenan, J.M., 2014. Partitioning of platinum-group elements and Au between sulfide liquid and basalt and the origins of mantle–crust fractionation of the chalcophile elements. Geochim. Cosmochim. Acta 125, 265–289.

Nagamori, M., Yazawa, A., 2001. Thermodynamic observations of the molten FeS–FeO system and its vicinity at 1473 K. Metall. Mater. Trans. B 32, 831–837.
O'Neill, H.S., 1991. The origin of the Moon and the early history of the Earth – a chemical model. 1. The Moon. Geochim. Cosmochim. Acta 55, 1135–1157.
O'Neill, H.S.C., Eggins, S.M., 2002. The effect of melt composition on trace element partitioning: an experimental investigation of the activity coefficients of FeO, NiO, CoO, MoO_2 and MoO_3 in silicate melts. Chem. Geol. 186, 151–181.
O'Neill, H.S.C., Mavrogenes, J.A., 2002. The sulfide capacity and the sulfur content at sulfide saturation of silicate melts at 1400 degrees C and 1 bar. J. Petrol. 43, 1049–1087.
Presnall, D.C., Dixon, S.A., Dixon, J.R., Odonnell, T.H., Brenner, N.L., Schrock, R.L., Dycus, D.W., 1978. Liquidus phase relations on join diopside–forsterite–anorthite from 1 am to 20 kbar – their bearing on generation and crystallization of basaltic magma. Contrib. Mineral. Petrol. 66, 203–220.
Rehkämper, M., Halliday, A.N., Fitton, J.G., Lee, D.C., Wieneke, M., Arndt, N.T., 1999. Ir, Ru, Pt, and Pd in basalts and komatiites: new constraints for the geochemical behavior of the platinum-group elements in the mantle. Geochim. Cosmochim. Acta 63, 3915–3934.
Ripley, E.M., Brophy, J.G., Li, C.S., 2002. Copper solubility in a basaltic melt and sulfide liquid/silicate melt partition coefficients of Cu and Fe. Geochim. Cosmochim. Acta 66, 2791–2800.
Robinson, J.A.C., Wood, B.J., Blundy, J.D., 1998. The beginning of melting of fertile and depleted peridotite at 1.5 GPa. Earth Planet. Sci. Lett. 155, 97–111.
Roy-Barman, M., Wasserburg, G.J., Papanastassiou, D.A., Chaussidon, M., 1998. Osmium isotopic compositions and Re–Os concentrations in sulfide globules from basaltic glasses. Earth Planet. Sci. Lett. 154, 331–347.
Salters, V.J.M., Stracke, A., 2004. Composition of the depleted mantle. Geochem. Geophys. Geosyst. 5, Q05B07.
Shimazaki, H., Maclean, W.H., 1976. Experimental study on partition of zinc and lead between silicate and sulfide liquids. Miner. Depos. 11, 125–132.
Tuff, J., Wood, B.J., Wade, J., 2011. The effect of Si on metal–silicate partitioning of siderophile elements and implications for the conditions of core formation. Geochim. Cosmochim. Acta 75, 673–690.
Vaajamo, I., Taskinen, P., 2011. A thermodynamic assessment of the iron-lead binary system. Thermochim. Acta 524, 56–61.
Wade, J., Wood, B.J., 2005. Core formation and the oxidation state of the Earth. Earth Planet. Sci. Lett. 236, 78–95.
Wagner, C., 1962. Thermodynamics of Alloys. Addison-Wesley, Reading, MA.
Wai, C.M., Wasson, J.T., 1977. Nebular condensation of moderately volatile elements and their abundances in ordinary chondrites. Earth Planet. Sci. Lett. 36, 1–13.
Wood, B.J., Blundy, J.D., 1997. A predictive model for rare earth element partitioning between clinopyroxene and anhydrous silicate melt. Contrib. Mineral. Petrol. 129, 166–181.
Wood, B.J., Kiseeva, E.S., Mirolo, F.J., 2014. Accretion and core formation: the effects of sulfur on metal–silicate partition coefficients. Geochim. Cosmochim. Acta 145, 248–267.
Wood, B.J., Halliday, A., Rehkamper, M., 2010. Volatile accretion history of the Earth. Nature 467, E6–E7.
Wood, B.J., Halliday, A.N., 2005. Cooling of the earth and core formation after the giant impact. Nature 437, 1345–1348.
Wood, B.J., Wade, J., Kilburn, M.R., 2008. Core formation and the oxidation state of the Earth: additional constraints from Nb, V and Cr partitioning. Geochim. Cosmochim. Acta 72, 1415–1426.
Wood, J.A., Hashimoto, A., 1993. Mineral equilibrium in fractionated nebular systems. Geochim. Cosmochim. Acta 57, 2377–2388.
Workman, R.K., Hart, S.R., 2005. Major and trace element composition of the depleted MORB mantle (DMM). Earth Planet. Sci. Lett. 231, 53–72.
Wriedt, H.A., Morrison, W.B., Cole, W.E., 1973. Solubility of silver in gamma-Fe. Metall. Trans. 4, 1453–1456.
Yoshiki-Gravelsins, K.S., Toguri, J.M., 1993. Oxygen and sulfur solubilities in Ni–Fe–S–O melts. Metall. Trans. B 24, 847–856.